



OPEN

Finite element modeling of active cracking in actively reinforced concrete pavement slab exposed to fluctuating temperature

Muhammad Kashif¹, Ahsan Naseem², Kennedy Chibuzor Onyelowe³✉, Muhammad Rizwan Riaz¹, Syed Saqib Mehboob⁴, Pieter De Winne² & Hans De Backer²

The continuously reinforced concrete pavement (CRCP) system grapples with challenges such as non-uniform transverse crack patterns and the need for substantial reinforcement. Field research on the Belgian CRCP sections along motorway E313 indicates that active cracking induced by partial surface saw-cuts consistently leads to transverse crack patterns. This study introduces an innovative modification to the CRCP: the actively reinforced concrete pavement design (ARCP). The ARCP leverages partial surface saw-cuts to reduce reinforcement needs by replacing continuous-length steel bars with partial-length counterparts. The main objective of the present study is to develop a 3D finite element (FE) model capturing the active cracking behavior of ARCP under realistic external temperature variations. Comparative analysis with CRCP considers early-age crack patterns, crack strain development, and the distribution of maximum steel stress for different steel ratios (0.67%, 0.75%, and 0.85%). FE simulation results align with field data, indicating that ARCP exhibits similar early-age cracking behavior to CRCP but with a significant 24 to 42% reduction in total reinforcement. This innovation presents a promising avenue for addressing CRCP challenges while optimizing material usage in pavement construction.

Keywords Active cracking, Partial surface saw-cuts, Advanced reinforced concrete slab, Finite element simulation

Active cracking underlies the technologically innovative modified configuration of the continuously reinforced concrete pavement slab (CRCP), an actively reinforced concrete pavement (ARCP) slab. This pavement design reduces the required reinforcement within the concrete slab by introducing partial-length reinforcing bars instead of continuous-length ones, strategically positioned over areas prone to active cracking¹. The development of the reinforcement design for the ARCP slab will depend on how well the active cracking method produces cracks at predetermined positions in the concrete slab. Sandwiching continuous-length steel bars between partial-length steel bars is primarily done to tightly clamp any potential new natural cracks that may emerge within active cracks^{2,3}.

It is widely acknowledged that early-age transverse crack patterns significantly influence the long-term performance of CRCP. Despite efforts to optimize design and construction variables, studies indicate that irregular crack patterns, including clusters of closely spaced cracks, persist^{4–9}. An alternative approach, the active crack control method, was implemented using automated tape insertion and saw cuts. Initially, the tape insertion into freshly laid concrete was used to induce active cracking in CRCP sections in the United States. However, this method was discouraged due to the concrete popping, which disrupts the construction process^{10–15}. Among the active crack control methods, the utilization of partial surface saw-cuts emerged as a highly effective approach for generating transverse cracks at predetermined locations within the CRCP slab^{5,8,16–18}.

The straight transverse crack growth from the partial surface saw-cuts in the Belgian CRCP sections effectively prevented the formation of cluster cracking. Field research on Belgian CRCP sections constructed along Motorway E313 revealed that almost 92% of all cracks appeared in close proximity to the saw cuts^{5,16}. This implies

¹Department of Civil Engineering, University of Engineering and Technology Lahore, Lahore, Pakistan. ²Department of Civil Engineering, Ghent University, Ghent, Belgium. ³Department of Civil Engineering, Kampala International University, Kampala, Uganda. ⁴Department of Civil Engineering, University of Engineering and Technology Taxila, Taxila, Pakistan. ✉email: kennedychibuzor@kiu.ac.ug

that the steel bars positioned continuously between these active cracks only need to accommodate approximately 8% of the total cracks. Despite the evident success of partial surface saw-cuts in achieving uniform cracking, the current Belgian CRCP design continues to employ the passive longitudinal reinforcement layout used between 1990 and 2012. Therefore, there is a pressing need to reconfigure the longitudinal reinforcement design of CRCP by incorporating the active cracking concept to eliminate the unnecessary placement of continuously placed steel bars. A detailed discussion of this method is presented in section “Active cracking in CRCP sections”.

Recent investigations into the optimization of longitudinal reinforcement in a 330 mm (13-inch) thick Continuously Reinforced Concrete Pavement (CRCP) slab have been undertaken by the Texas Department of Transportation and the Federal Highway Administration¹⁹. The research comprised two distinct phases: (1) numerical modeling of CRCP, and (2) field experimentation. During the initial phase, the ANSYS Finite Element package scrutinized CRCP responses under environmental loading through three-dimensional modeling. In the subsequent phase, extensive field testing was carried out to explore the impacts of different longitudinal steel depths on CRCP responses, particularly focusing on concrete stresses leading to cracking. Field investigations revealed that the configuration of reinforcements in CRCP, specifically the depth of steel, significantly influences transverse cracking. The numerical model adopted a linear elastic and isotropic assumption, neglecting young hardening properties, and did not incorporate non-linear transient and structural analysis parameters to simulate the induction of transverse cracks in the CRCP slab. Another recent study has been conducted to develop a 3D numerical model using ABAQUS software for simulating the early-age cracking behavior of CRCP and ARCP. However, in this study, the critical consideration of young hardening concrete properties, including the simultaneous evolution of mechanical properties and stresses concerning the degree of hydration, has been omitted. These properties are crucial for accurately simulating early-age cracking in the concrete slab. Additionally, the model does not account for partial surface saw cuts to induce active cracks at the saw cut in the ARCP slab⁹.

The existing body of literature underscores the scarcity of research studies dedicated to developing a 3D finite element (FE) model aimed at replicating the early-age cracking tendencies of the ARCP slab employing partial surface saw-cuts under varying environmental loads. Thus far, investigations exploring the impacts of different steel ratios, varying steel bar diameters and spacings, the continuous fluctuations in environmental temperature, and the evolving properties of young hardening concrete on early-age cracking within ARCP slabs have been notably lacking. The main objective of the present study is to develop a rational design concept for ARCP through partial surface saw-cuts and compare it with the conventional design of CRCP currently practiced in the field. For this purpose, a 3D thermo-mechanical FE model that considers the nonlinear transient heat transfer analysis of cement hydration reaction and associated temperature development, in addition to the nonlinear structural analysis of stress and cracking development with respect to time, is developed for accurate simulation of early-age cracking in the concrete slab, starting from the time of concrete placement up to thirty days. In advance of the extremely costly experimentation required to investigate the behavior of concrete pavement, the findings of the present research might be useful in developing a rational design of the ARCP slab employing partial surface notches.

Research significance

The literature emphasizes that the inventive idea of the ARCP slab using partial surface saw-cuts has not yet been implemented in practice. Therefore, understanding the mechanism that causes early-age crack induction in the ARCP slab and assessing the effect of significant factors such as steel ratio, steel bar diameter, and steel bar spacing on the cracking characteristics of the ARCP slab under fluctuating temperature conditions are vitally required to develop the reinforcement design layout of the ARCP. The developed 3D FE model is suggested as a tool to evaluate the longitudinal reinforcement design layout of the ARCP slab in advance of field construction and choose a cost-efficient reinforcement design.

Active cracking in CRCP sections

In 2012, a deliberate approach involving partial surface notches was employed at a distance of 1200 mm to intentionally generate transverse cracking at specific locations within the Belgian CRCP sections at motorway E313, as shown in Fig. 1^{5,16}. This experimental setup incorporated two different saw-cut depths—60 mm and 30 mm—to investigate the influence of partial surface notch depth on the formation of cracks at the predetermined positions, namely the saw-cut locations, within the CRCP slab. A straight and uniform transverse crack pattern was produced in the E313 CRCP section, as shown in Figs. 2 and 3. The effectiveness of this active crack control approach to cause active cracking in the CRCP section is shown in Table 1. Notably, within the first four days following the concrete placement, it was observed that 99% of all cracks emerged precisely over the saw-cut positions within the CRCP test section featuring a 60 mm notch. Out of the 664 cracks, 555 cracks appeared at the saw-cut locations after 65 days^{5,16}. Nearly 92% of all cracks were located between 0 and 0.4 m from the notches after a year. Only 8% of all cracks extended beyond 0.4 m from the notches. This value increases to 17.3% in the CRCP section containing a 30 mm notch, as shown in Table 1. Inducing straight and uniform transverse cracks from partial surface notches in the CRCP slab has reportedly been shown to be more successful with a deeper notch than a shallower one⁵.

Inspired by the experiences with active cracking in the Belgian CRCP sections, the field research was conducted involving the construction of three CRCP sections, denoted as sections “Introduction”, “Research significance”, and “Active cracking in CRCP sections”, along Illinois Route 390 in the United States^{8,18}. In this investigation, sections “Introduction” and “Active cracking in CRCP sections” were constructed with partial surface notches that were 600 mm long (2 feet) and 50 mm (2 inches) deep, spaced at intervals 1200 mm (4 feet) as shown in Fig. 4. For comparison purposes, section “Research significance” was constructed without the partial surface notches, while section “Active cracking in CRCP sections” was built with the partial surface notch and

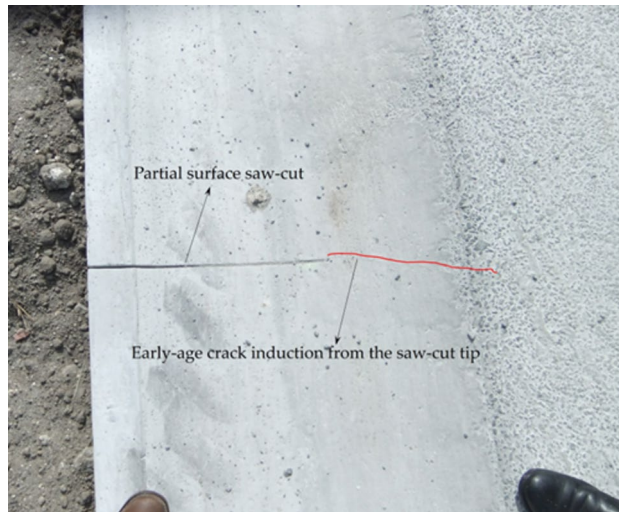


Figure 1. Partial surface saw-cut in the CRCP slab at motorway E313.

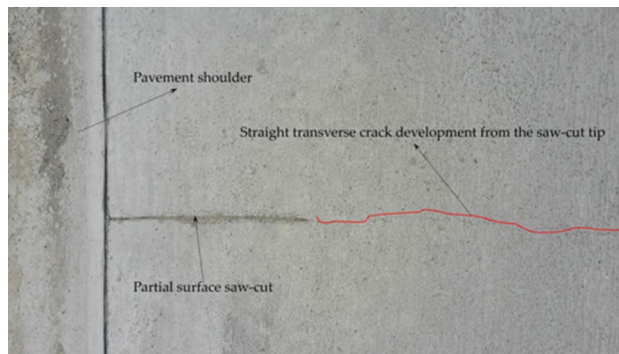


Figure 2. Straight transverse crack formation from the saw-cut tip in the E313 CRCP section.

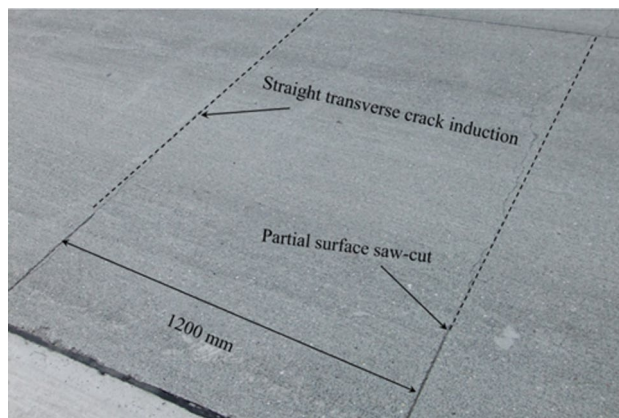


Figure 3. A straight and uniform transverse crack pattern in the CRCP section at motorway E313.

internal curing to induce active cracking. In the internal curing process, prewetted fine lightweight aggregates with an absorption capacity of 10.5% replaced around 37% of the volume of fine aggregate. A straight and uniform transverse crack pattern was observed in section “Active cracking in CRCP sections”, as depicted in Fig. 5. The percentage of active crack induction with respect to time from the partial surface notch is shown in Fig. 6. Approximately 85% of the total cracks emerged from the partial surface saw-cuts after 3 years. This implies that only 15% of total cracks are passively induced in the pavement slab. It was also reported that about 93% of total

| Road section | Length (m) | Age (Days) | No. of notches (N1) | No. of cracks (N2) | No. of cracks at notches (N3) | Effectiveness of notches N3/N1 (%) | Percentage of cracks in category by distance to nearest notch (m) | | | |
|---------------------|------------|------------|---------------------|--------------------|-------------------------------|------------------------------------|-------------------------------------------------------------------|-------|---------|---------|
| | | | | | | | 0 | 0–0.2 | 0.2–0.4 | 0.4–0.6 |
| 60-mm saw-cut depth | 1100 | 4 | 897 | 193 | 191 | 21.3 | 98.9 | 0 | 0 | 1.1 |
| | 1100 | 65 | 897 | 664 | 555 | 61.9 | 83.5 | 2.4 | 7.7 | 6.4 |
| | 1100 | 204 | 897 | 762 | 597 | 66.6 | 78.4 | 3.8 | 9.8 | 8.0 |
| | 1100 | 378 | 897 | 775 | 606 | 67.6 | 78.2 | 3.8 | 9.9 | 8.1 |
| | 500 | 123 | 422 | 417 | 245 | 58.1 | 58.7 | 9.4 | 15.9 | 16.0 |
| 30-mm saw-cut depth | 500 | 262 | 422 | 497 | 281 | 66.5 | 56.5 | 8.7 | 17.5 | 17.3 |
| | 500 | 436 | 422 | 502 | 285 | 67.5 | 56.8 | 8.6 | 17.3 | 17.3 |

Table 1. Effectiveness of partial surface saw-cuts to produce active cracking in CRCP section ⁵.



Figure 4. Early entry partial surface saw cut made in the CRCP slab in Illinois, United States ¹⁸.



Figure 5. Straight crack propagation from saw-cuts in the CRCP section ¹⁸.

cracks (193 out of 207 cracks) originated from the partial surface notches and 7% of total cracks (7 out of 207 cracks) were naturally (passively) induced in the CRCP section ^{8,18}.

Details of finite element modeling

Model geometry

The 3D FE model incorporates the geometric configurations of CRCP, following the current Belgian design standard for CRCP. As indicated in Fig. 7, the 20 mm diameter longitudinal steel bars are positioned 170 mm apart and 80 mm below the top of the concrete slab. The pavement lane width of 3600 mm is assumed in this study ⁵. The response of the CRCP slab under environmental load is presumptively symmetrical regarding the middle of the pavement lane and the two successive transverse cracks ^{6,17,20–27}. Considering anticipated symmetry in the response of the CRCP slab to environmental loading, computational efficiency is enhanced by modeling both sides of the saw cut, along with the corresponding half of the road lane, thereby reducing computational time and storage requirements.

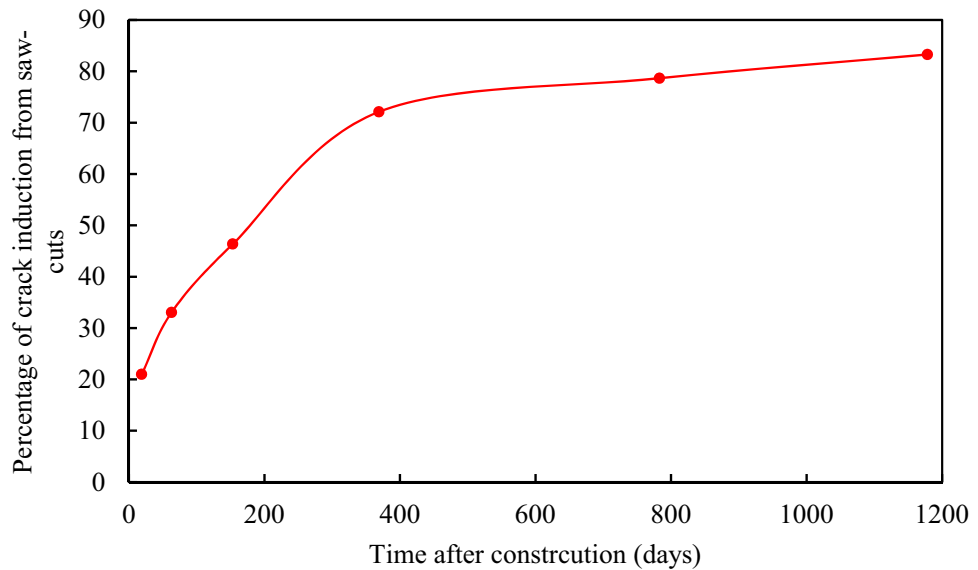


Figure 6. Influence of the partial surface saw-cut on the progression of crack formation¹⁸.

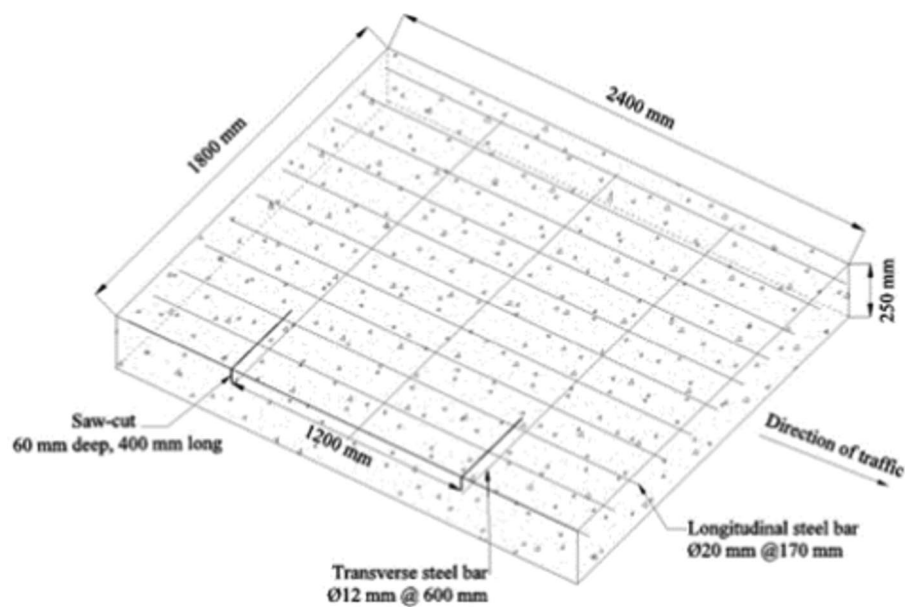


Figure 7. Reinforcement details of the CRCP segment.

Analysis type

The 3D staggered structural-flow analysis is carried out to mimic the early-age active cracking in the CRCP slab exposed to changing temperature fields shown in Fig. 8. This analysis consists of two distinct phases. The initial phase, the nonlinear transient heat flow analysis, focused on predicting temperature variations within the concrete slab and transforming structural components into flow elements. The thermal strain data obtained from the first phase were utilized as thermal load inputs for the subsequent phase, known as the nonlinear structural analysis. These two phases were interconnected²⁸. This type of analysis requires knowledge of concrete's thermo-mechanical characteristics, such as heat capacity, thermal expansion coefficient, thermal conductivity, and mechanical properties evolution. There are various young hardening constitutive models for concrete in the DIANA FE program. The EN 1992-1-1 model in the DIANA material library is used to determine the fundamental properties of hydrating concrete in this research.

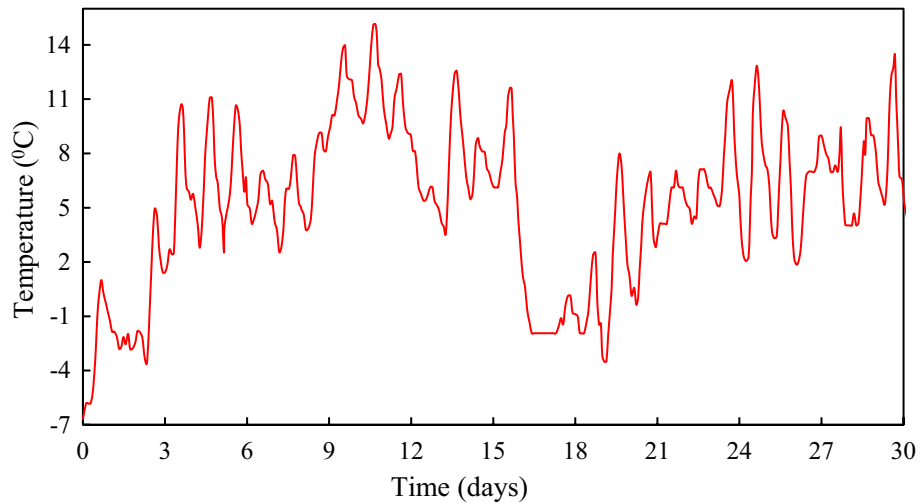


Figure 8. Varying external air temperature loading.

Constitutive model

Within the FE program, the maturity variable is employed to characterize the progression of cement hydration, denoted as the degree of reaction (r). Equation (1) defines this variable as the ratio of the cumulative total heat generated up to time t to the cumulative total heat of hydration over 28 days. The heat generation is intricately linked to the temperature history. The instantaneous rate of heat production denoted as $q(r, T)$ is defined by Eq. (2). Where, r represents the degree of reaction ($0 \leq r \leq 1$), while T signifies the temperature, and α is the maximum rate of heat production. In this equation, q_r and q_T correspond to the heat production rates that are contingent on the degree of reaction and temperature, respectively. The temperature-dependent component of heat production is calculated through Eq. (3). Where C_A denotes the Arrhenius constant, the magnitude of which is dependent on the temperature and/or the degree of reaction. This particular constant plays a crucial role in the computations carried out by DIANA pertaining to heat generation and the determination of equivalent age²⁸. The heat generation $q(t)$ is calculated by the DIANA FE package using Eq. (4). In this equation, $c(T, r)$ signifies the heat capacity, which can assume either a constant value or vary as a function of both temperature and the degree of reaction. The thermal conductivity (k), governing heat conduction, can remain constant or vary with dependencies on temperature and the degree of reaction, as detailed in Eq. (5). Where, $q(\text{cond})$ stands for the conductive heat flux.

$$r = \frac{\int_0^t q(r, T) dT}{\int_0^{28} q(r, T) d\tau} \quad (1)$$

$$q(r, T) = \alpha \cdot q_r(r) \cdot q_T(T) \quad (2)$$

$$q_T(T) = e\left(-\frac{C_A(r, T)}{T}\right) \quad (3)$$

$$q(t) = c(T, r) \frac{\partial T}{\partial t} \quad (4)$$

$$q(\text{cond}) = -k(r, T)(\nabla T) \quad (5)$$

The DIANA FE program utilizes the maturity variable (r) to compute the hydration heat, temperature development, and evolution of concrete mechanical properties^{28,29}. The progress of heat development in concrete is described by characterizing an adiabatic heat curve based on the validated heat of hydration, especially applicable to blast furnace slag cement³⁰. The evolution of compressive strength is articulated by Eq. (6). In this equation, f_{cm28} denotes the average compressive strength achieved at the 28-day mark, while $\beta_{cc}(t)$ represents a time-dependent coefficient, the calculation of which is delineated in Eq. (7). The value of s is dependent on the specific type of cement employed. The parameter t_{eq} corresponds to the equivalent age and is derived through the application of Eq. (8), wherein T_{ref} designates a reference temperature, and T_t signifies the concrete temperature at t days. The evolution of Young's modulus for concrete, denoted as $E_{cm}(t)$ at a given age of t days is detailed in Eq. (9). Equation (10) describes the evolution of the tensile strength $f_{ctm}(t)$ as a function of time^{28,29}.

$$f_{cm}(t) = \beta_{cc}(t) f_{cm28} \quad (6)$$

$$\beta_{cc}(t) = \exp\left(s\left(1 - \sqrt{\frac{28}{t_{eq}}}\right)\right) \quad (7)$$

$$t_{eq} = \int_0^t \exp\left(C_A\left(\frac{1}{T_{ref}} - \frac{1}{T_t}\right)\right) dt \quad (8)$$

$$E_{cm}(t) = \left(\frac{f_{cm}(t)}{f_{cm28}}\right)^{0.3} E_{cm28} \quad (9)$$

$$f_{ctm}(t) = \beta_{cc}(t)f_{ctm28} \quad (10)$$

Model input parameters

Constant values for the specific heat and thermal conductivity of concrete are utilized to estimate the early-age temperature development due to challenges associated with calculating the thermal properties of concrete at this stage. A crucial parameter indicative of volumetric changes in concrete is the coefficient of thermal expansion (CTE). As aggregates constitute a significant portion, ranging from 70 to 85% of the concrete's solid volume, the CTE is significantly influenced by the aggregate type and mineral composition. To ascertain the CTE of early-age concrete, numerous experimental studies have been conducted. It has been reported that CTE increases before reaching its final setting and subsequently stabilizes at a constant value. The initial high CTE of concrete is ascribed to unreacted water, given that the CTE of water is 20 times higher than that of other concrete components. Therefore, it is recommended to use a constant CTE value after the concrete reaches its final setting when predicting thermal stress development^{5,21,31–38}. Experimental results for the CTE of concrete at the Belgian motorway E17 are shown in Table 2. These findings have informed the decision to utilize a constant CTE value in the FE simulation, with the input properties comprehensively presented in Table 3.

Model boundary conditions and meshing

The model's boundary conditions account for both components of the staggered structural-flow analysis discussed earlier. In the context of nonlinear structural analysis, the lower surface of the concrete slab is assumed to be translationally fixed in the upward direction, considering a more rigid underlying ground base underneath the slab. Conversely, the outer edge of the slab, located above the notch side, is permitted to expand, and contract in response to varying external temperature fluctuations. Due to the infinity of surrounding concrete, translational movements of the lateral faces in the Y–Z plane are constrained in the slab's longitudinal direction. At the symmetry line of the lane center, translational restrictions are applied to the end face of the slab in the slab's transverse direction. The contact interface between the lower surface of the concrete slab and the underlying

| Specimen | CTE (10 ⁻⁶ mm/mm/°C) | | |
|----------|---------------------------------|--------------|--------------|
| | Test cycle 1 | Test cycle 2 | Test cycle 3 |
| CTE-1 | 11.3 | 11.3 | 11.3 |
| CTE-2 | 11.0 | 11.0 | 11.0 |
| CTE-3 | 10.0 | 10.0 | – |

Table 2. Measured values of CTE of concrete used at motorway E17⁹.

| | |
|----------------------------------------------------------------------------------------|-------------------------|
| Concrete class | C45/55 |
| Aggregate type | Limestone |
| Thermal expansion coefficient of concrete (1/°C) | 10.0 × 10 ⁻⁶ |
| Thermal conductivity of concrete (W/m °C) | 2.7 |
| Heat capacity of concrete (J/m ³ °C) | 2.87 × 10 ⁶ |
| Coefficient of convection and radiation between concrete and air (W/m ² °C) | 7.55 |
| Initial temperature (°C) | 20 |
| Slab notional size (mm) | 439 |
| Relative humidity (%) | 80 |
| Curing age (Days) | 3 |
| Steel's modulus of elasticity (GPa) | 200 |
| Steel's yield strength (MPa) | 500 |

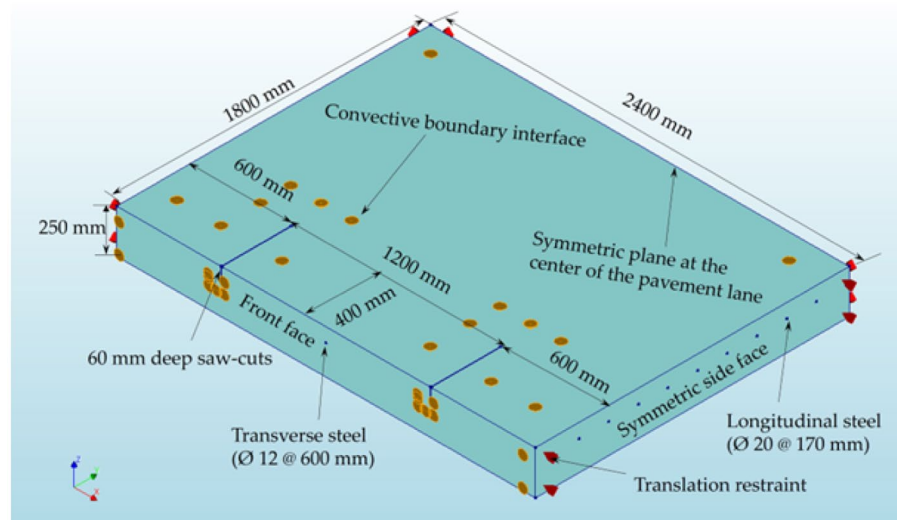
Table 3. Model input parameters.

ground base is characterized by a nonlinear elastic friction model, simplifying the Coulomb friction model^{36,39,40}. Equation (11) illustrates the constitutive behavior of this interface model in the elastic regime. The yield function, described by Eq. (12), governs yielding in this model, with the effective shear stress (τ) being determined as $\sqrt{t_s^2 + t_t^2}$, where t_s and t_t denote shear tractions, while s and t correspond to traction axes parallel to the interface element's plane.

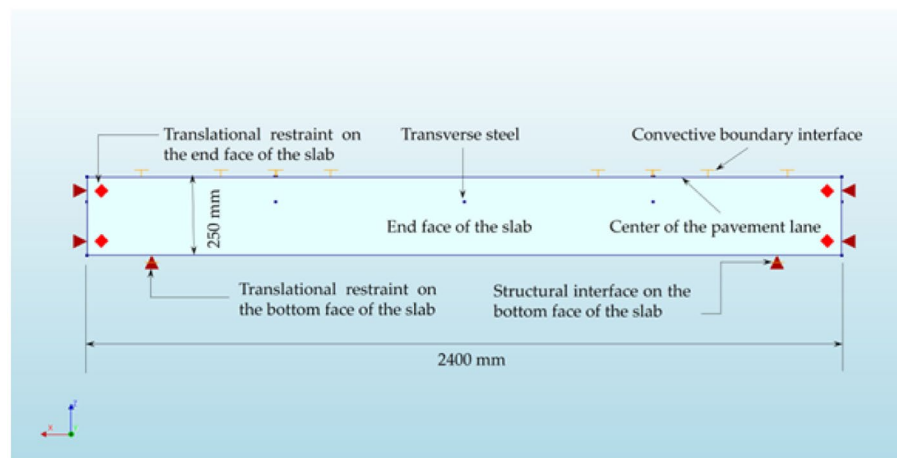
$$t = D^e u \quad (11)$$

$$|\tau| + t_n \tan \theta - c = 0 \quad (12)$$

For non-linear heat analysis, the upper and outer surfaces of the slab are directly subjected to fluctuating external temperature conditions as depicted in Fig. 9. Convective boundary interface elements are used to describe the heat transfer occurring between these exposed concrete surfaces and the surrounding environment. Newton's law of cooling, which is illustrated in Eq. (13), governs the convective heat exchange taking place at these surfaces. Consistent with existing literature^{5,26,36,37,40–42}, a heat transfer coefficient of $7.55 \text{ W/m}^2 \text{ } ^\circ\text{C}$ is applied to the thermal boundary interface elements. A 20-node brick element called CHX60 is used to discretize the concrete material. The convective interface boundary between the exposed slab areas and the outside environment is described through a four-node isoparametric quadrilateral element (BQ4HT). For the contact interface between the concrete slab and the underlying ground base layer, an eight-node interface element denoted as CQ481, characterized by zero thickness, has been employed. Figure 9 illustrates the boundary conditions for the FE model. The reinforcing steel bars are modelled as embedded reinforcement with their behavior defined as elastoplastic



(a)



(b)

Figure 9. The boundary conditions of the active crack control CRCP slab (a) 3D view (b) End face view.

without any consideration for hardening phenomena. The full bonding contact between concrete and steel is assumed to facilitate smooth convergence during the 3D analysis and to reduce computational calculations²².

The results of the FE simulation rely on the choice of element size and type during the meshing process. To address this, a mesh sensitivity analysis is conducted, employing four distinct element sizes: 10 mm, 20 mm, 30 mm, and 60 mm, to identify the most optimal element size. Figure 10 illustrates the impact of element size on the evolution of total strain over time. This figure clearly indicates that there is no noticeable difference in total strain values between mesh sizes of 20 mm and 30 mm. As a result, for the current investigation, a mesh size of 30 mm is chosen to mesh the CRCP model. Figure 11 provides a closer look at the finer mesh zone enveloping the partial surface notches within the CRCP slab. The flowchart of the research methodology is shown in Fig. 12.

$$q(conv) = h_c k(T_s - T_e) \tag{13}$$

Model validation

Partial surface saw-cuts are purposely employed in Belgian CRCP sections to produce active cracking. This strategy aims to ensure a consistent and straight propagation of cracks across the width of the pavement, a phenomenon substantiated by field observations exemplified in Figs. 2 and 3. The early-age cracking behavior of the Belgian CRCP section at motorway E313 is used as field evidence to validate the 3D FE model. Figure 12 presents a graphical representation of the evolution of tensile stress versus developing tensile strength along the CRCP

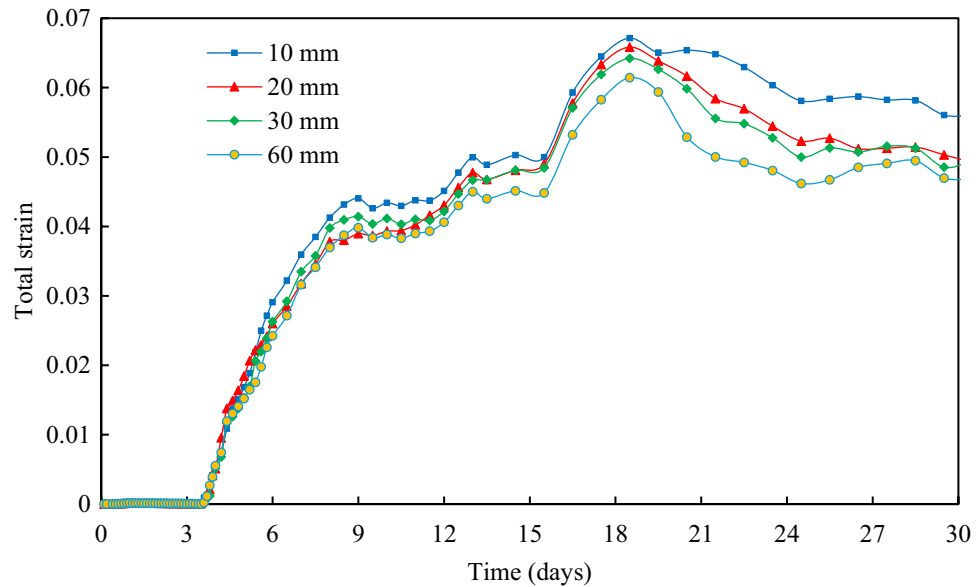


Figure 10. Illustration of the impact of element size on total strain evolution at the saw-cut tip.

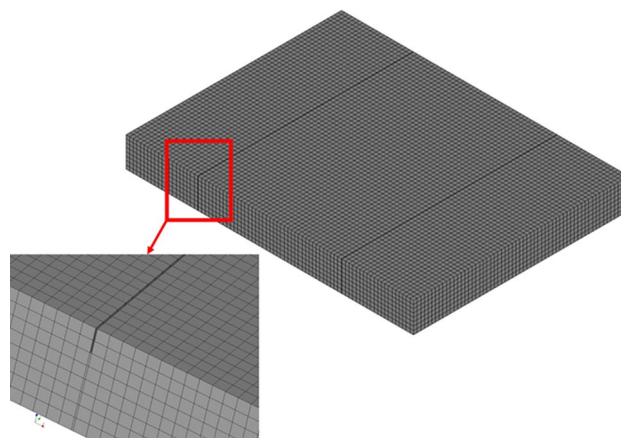


Figure 11. Refined meshing around the saw cut in the CRCP slab.

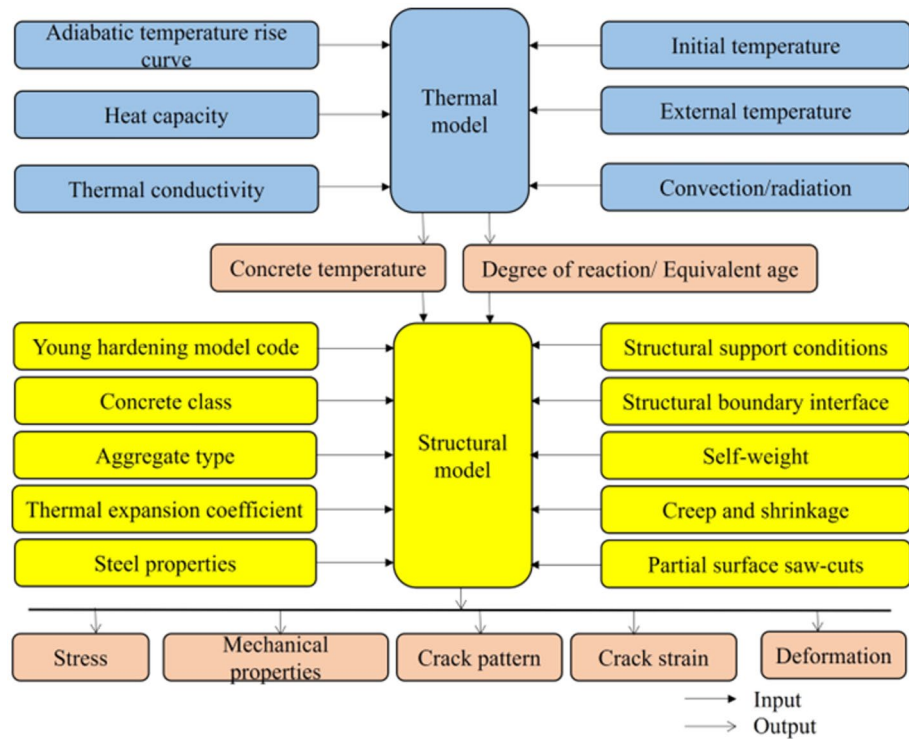


Figure 12. Flow chart of the research methodology.

segment’s length across the notch tips to predict the crack initiation locations. As Fig. 13 illustrates, the tensile stress at the notch tips surpasses the evolving concrete tensile strength, leading to crack initiation at these precise locations, as shown in Fig. 14. Subsequent crack progression over time, originating from these saw-cut tips, is indicated in Figs. 15 and 16. Since the stress values between the saw cuts are less than the tensile strength, no cracking develops in the areas between the cuts. “Eknn” in Figs. 14, 15, and 16 represents crack strain values. It is evident that the predictions of the 3D FE model closely align with the actual observations of the transverse crack pattern’s development in the CRCP section at motorway E313, as illustrated in Fig. 3.

Figure 17 illustrates the evolution of maximum steel stress within the third longitudinal steel bar positioned directly ahead of the notch, providing insight into stress fluctuations. Significantly, stress peaks precisely coincide with the locations of notch tips, where crack initiation occurs. Between these notch tips, stress values diminish

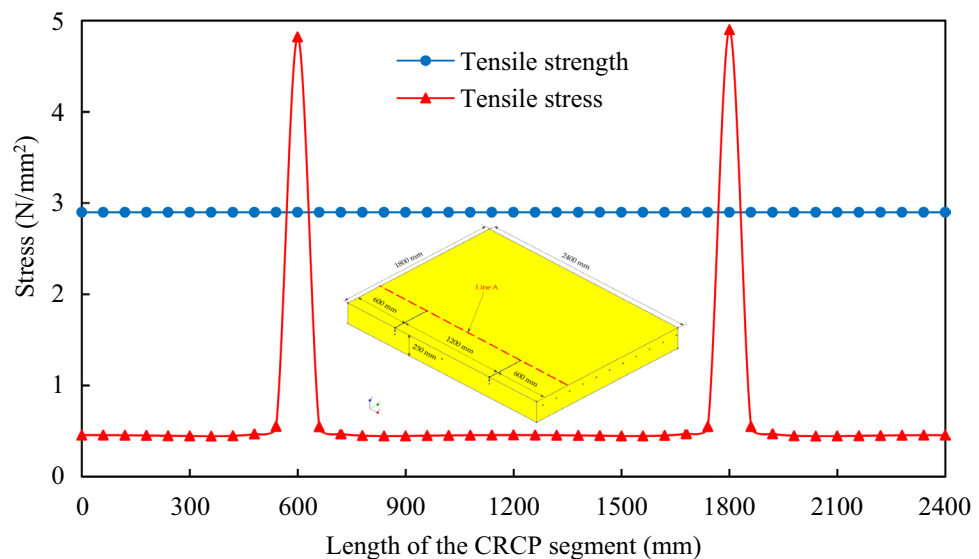


Figure 13. Comparison of the evolution of concrete tensile strength with the maximum tensile stress development along the CRCP slab’s length (at line A) after 3.5 days.

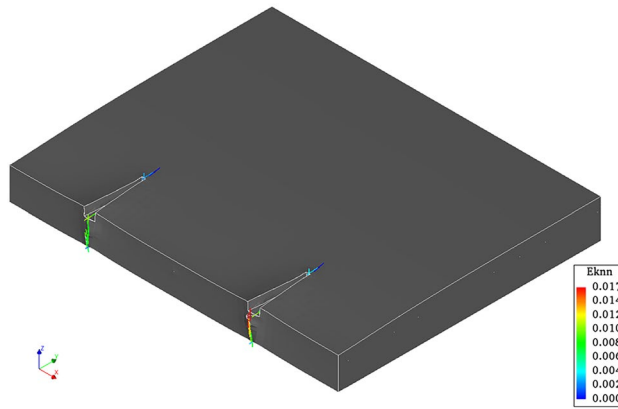


Figure 14. Initiation of cracks at notch tips after 90 h.

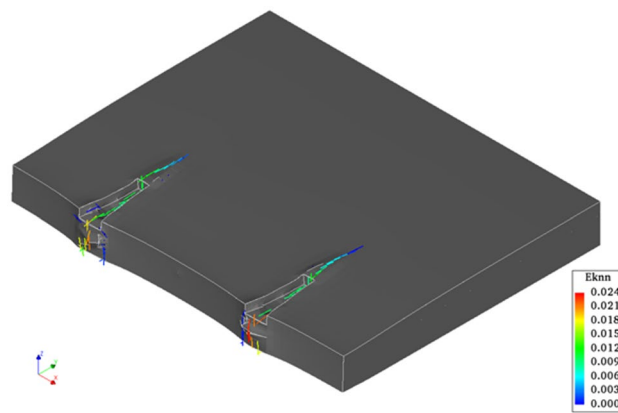


Figure 15. Crack propagation after 100 h.

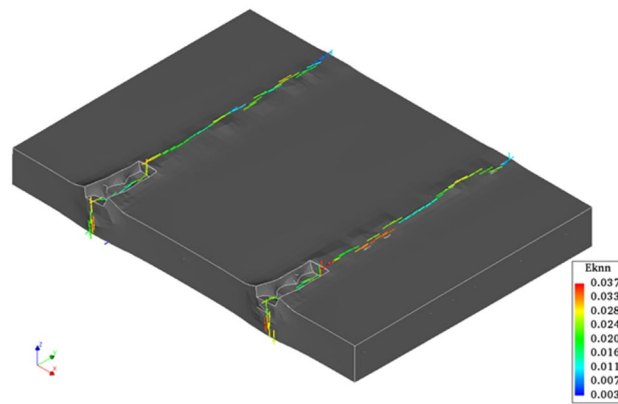


Figure 16. Formation of transverse crack pattern after 144 h.

to zero. This steel stress profile indicates that, in the absence of passive cracking, the continuous longitudinal steel bars in the slab are not necessary elsewhere except at the locations of active cracks. To develop the reinforcement design for the ARCP slab, the superfluous continuous steel bars between active cracks are substituted with partial steel bars. The 3D FE model developed, considering concrete tensile stress development, transverse crack initiation, and steel stress profiles, is expected to effectively simulate early-age cracking in CRCP under fluctuating temperature conditions.

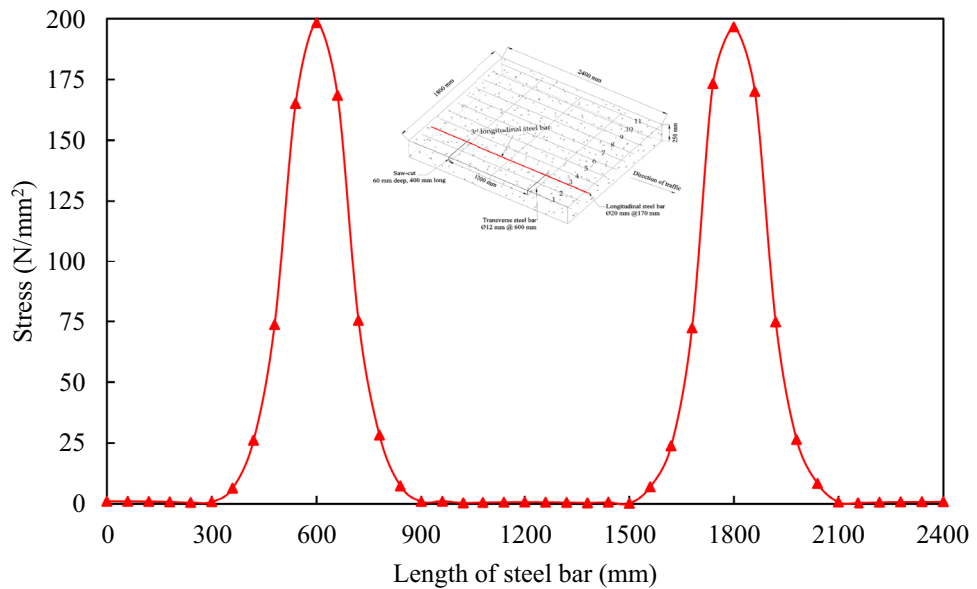


Figure 17. Illustration of the evolution of the highest stress experienced by the third continuous longitudinal steel bar.

Partial steel bars in the ARCP design

The design of the reinforcement layout for ARCP slabs depends on several key factors: the efficacy of partial surface notch in generating cracks at specific locations, the attainment of maximum stress levels in the continuously placed steel bar, and the precise spacing of the saw-cuts in accordance with the design parameters. As previously discussed, field experience of active cracking induced by partial surface saw-cuts has revealed that approximately 92% of all cracks originate directly over saw-cut sites. This indicates that the amount of continuous reinforcement needed to accommodate 100% passive cracks significantly exceeds what is necessary for the remaining 8%. To mitigate the need for an excessive quantity of continuous longitudinal steel bars, a viable approach is partial replacement with partial steel bars, as demonstrated in Figs. 18 and 19. In this context, an ARCP slab with a single consecutive replacement of continuous steel bars is designated as ARCP-1, and one with two consecutive replacements is denoted as ARCP-2. The behavior of the ARCP slab, with respect to the initiation and propagation of crack from the notch tips, closely resembles that of the CRCP slab, as evidenced by Figs. 20 and 21, mirroring the findings presented in Figs. 14, 15, and 16.

The evolution of crack strain over time at the notch tips, as depicted in Fig. 22, provides insights into the effectiveness of a 600 mm-long partial steel bar in controlling active cracking. This is evidenced by the gradual reduction in steel stress values to zero at 300 mm from the axis of the partial surface saw cut. Figure 22 reveals that there are no substantial variations in crack strain values among CRCP, ARCP-1, and ARCP-2. Figure 23 presents a comparative analysis of the maximum stress evolution in the third longitudinal steel bar of the CRCP slab and that of ARCP-1 and ARCP-2. As illustrated in Fig. 23, the partial steel bar demonstrates equivalent steel stress development to that of the continuous steel bar. These findings suggest that the partial steel bar can be effectively employed in active crack areas as a substitute for continuous steel bars. However, for maintaining the

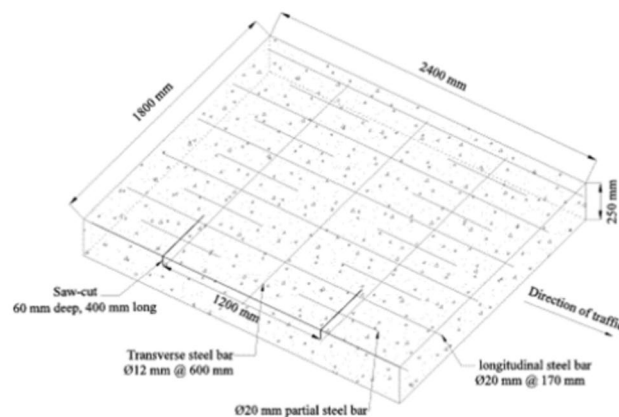


Figure 18. Configuration of reinforcement in ARCP-1.

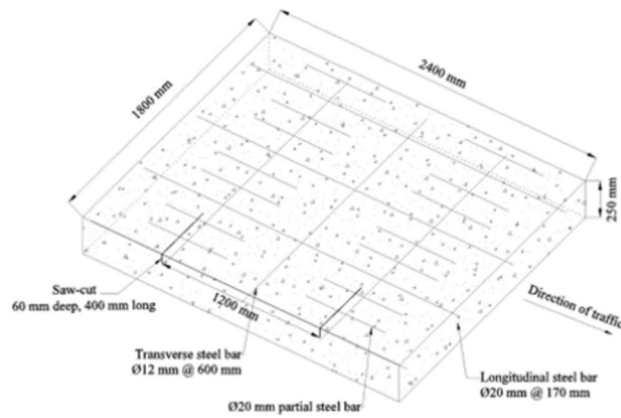
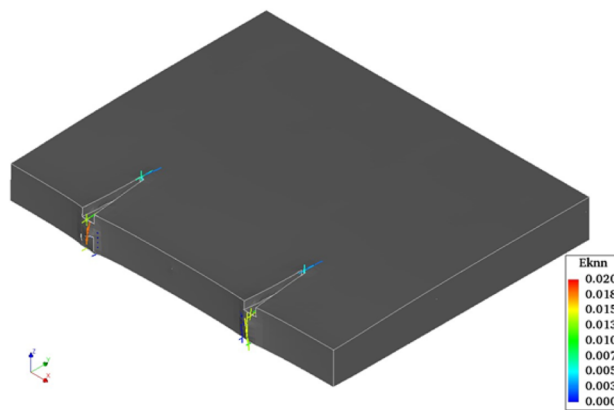
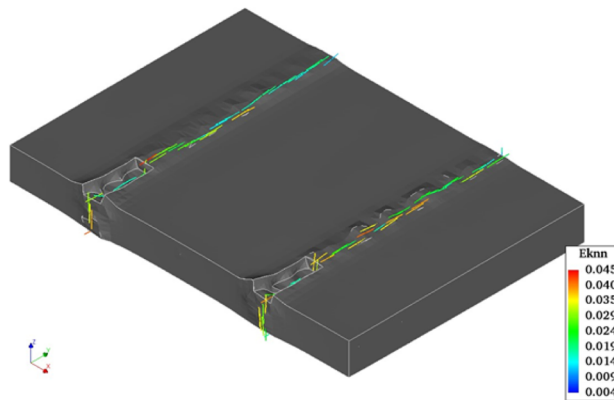


Figure 19. Configuration of reinforcement in ARCP-2.



(a)



(b)

Figure 20. Active cracking in ARCP-1 (a) Crack induction after 90 h (b) Crack propagation after 144 h.

structural integrity of the pavement, continuous steel bars remain indispensable in passive crack areas. The 3D FE model for assessing the reinforcement design of the ARCP slab takes into account three distinct longitudinal reinforcement ratios (0.67%, 0.75%, and 0.85%), two steel bar diameters (16 mm and 20 mm), and three steel bar spacings (170 mm, 100 mm, and 95 mm). A comprehensive evaluation of the feasibility of substituting partial-length bar steel with continuous-length bar steel at active cracking areas in the concrete slab, while considering various reinforcement ratios, bar diameters, and spacing, necessitates a thorough parametric analysis.

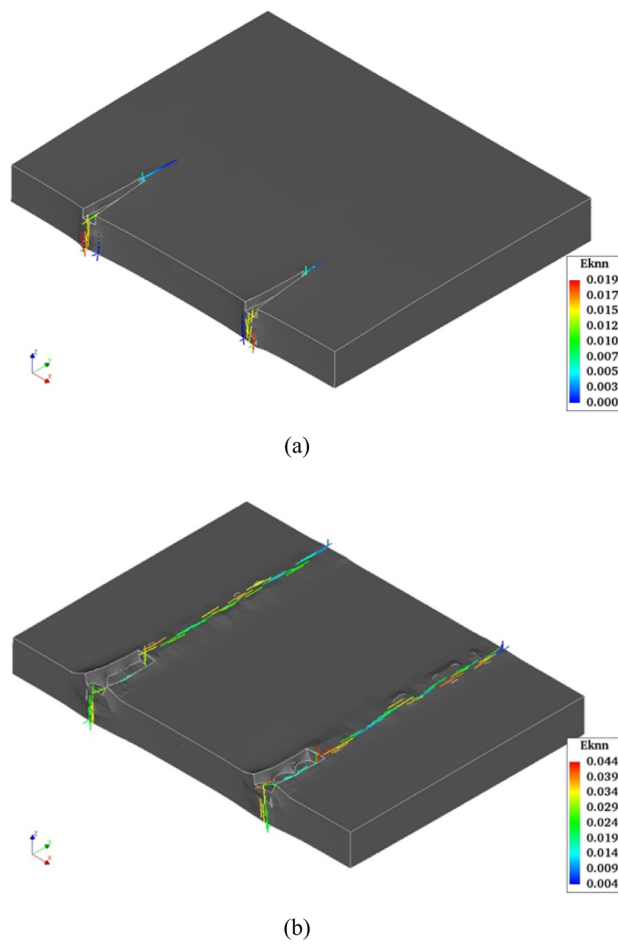


Figure 21. Active cracking in ARCP-2 (a) Crack induction after 90 h (b) Crack propagation after 144 h.

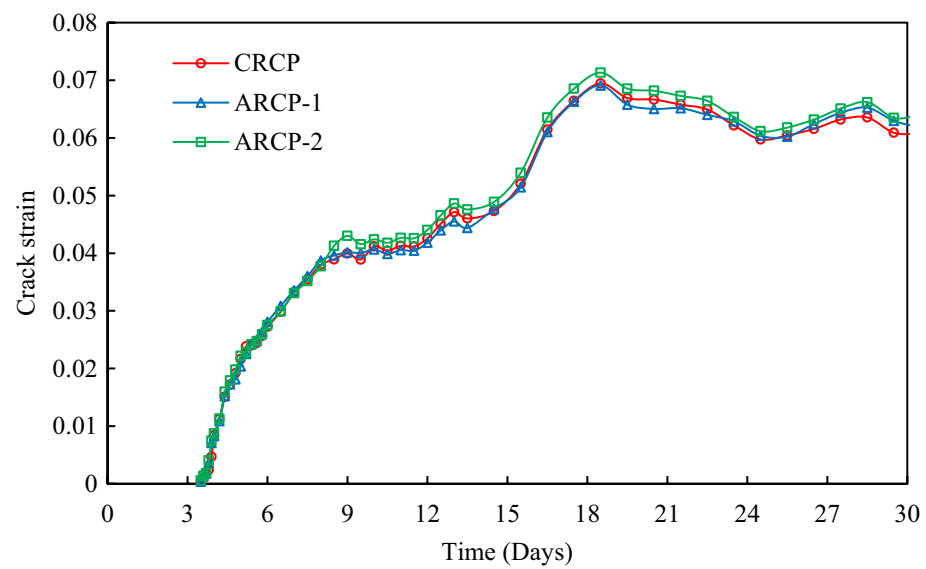


Figure 22. Comparing crack strain evolution over time at the notch tip: a comparative assessment involving CRCP, ARCP-1, and ARCP-2.

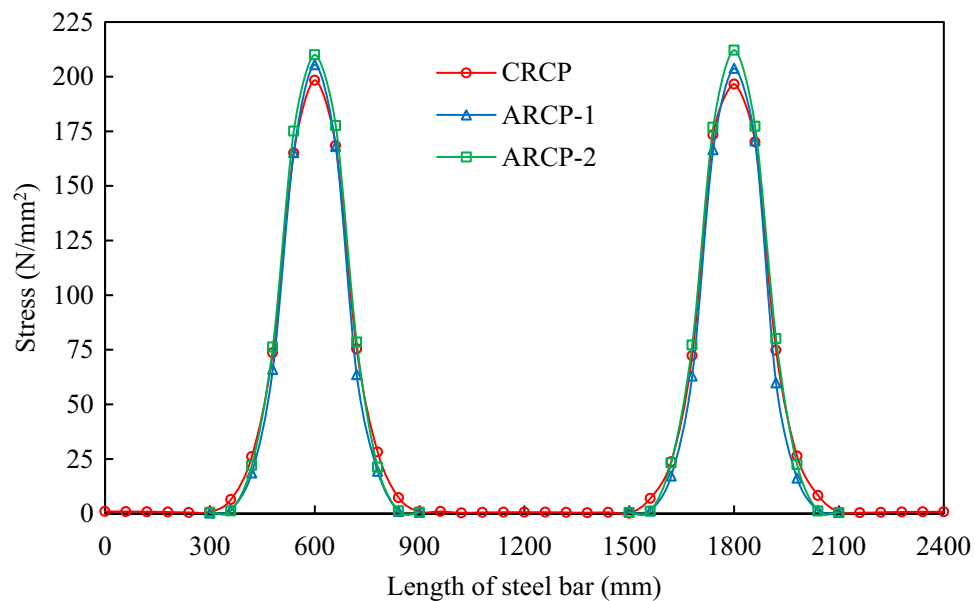


Figure 23. The peak stress development in the first partial-length bar of ARCP-1, ARCP-2, and the equivalent second continuous-placed bar of CRCP.

Parametric evaluation

The present study involves a parametric evaluation of the longitudinal reinforcement layout for the ARCP, considering different longitudinal reinforcement ratios (0.67%, 0.75%, and 0.85%) and two steel bar diameters (16 mm and 20 mm). Each reinforcement layout is assessed based on the crack strain evolution over time. A comparison of the ARCP slab is also made with the CRCP slab regarding the total amount of longitudinal reinforcement. Due to the inherent passive tendency of pavement slab cracking, earlier reinforcement layouts of the Belgian CRCP have been altered by adjusting the reinforcement ratio from 0.67 to 0.85%. Field observations of the CRCP test sections constructed with various reinforcement ratios have shown that the incidence of cracking increases with an increasing reinforcement ratio^{5,16,43–46}. As there are no transverse joints provided in this pavement system for stress relief, a larger reinforcement ratio increases restraint against volume variations in concrete induced by environmental loading, which in turn increases cracking incidence in the CRCP slab. For example, CRCP sections built following design concept-2 with a 0.67% reinforcement ratio exhibited a more consistent crack pattern than those constructed by design concept-1 with a 0.85% reinforcement ratio⁵.

ARCP is an innovative rigid pavement structure that necessitates an optimized reinforcement layout design for the placement of partial steel bars and continuous steel bars before performing costly field trials. Two basic configurations (ARCP-1 and ARCP-2) of the ARCP following the Belgian CRCP design concept-3 are discussed in section “[Partial steel bars in the ARCP design](#)”. Both configurations have been adjusted using 16 mm diameter steel bars ($\varnothing 16$), as depicted in Fig. 24, to evaluate their impact on the progression of crack strain at the notch tips. As observed, when employing smaller diameter steel bars, the number of continuous steel bars increases while maintaining the same reinforcement ratio. Figure 25 provides a comparative analysis of the crack strain evolution over the notch tips for ARCP-1 and ARCP-2, both featuring a reinforcing ratio of 0.75%. Notably, the employment of 16 mm diameter ($\varnothing 16$) steel bars results in a substantial reduction in crack strain for both ARCP-1 and ARCP-2. Additionally, it is important to highlight that, for an equivalent reinforcement ratio, ARCP structures with fewer continuous steel bars induce higher crack strain values than those equipped with a greater number of continuous steel bars. This trend can be attributed to the presence of more longitudinal steel bars with smaller diameters, contributing to a reduction in crack strain at the transverse crack interface.

Table 4 provides a comparative analysis of reinforcement layout details for CRCP, ARCP-1, and ARCP-2, all designed with a 0.75% reinforcement ratio. This table provides a clear visual representation of the significant advantages offered by ARCP-1 and ARCP-2 when employing a 16 mm steel bar, showcasing a remarkable reduction in reinforcement amount as compared to traditional CRCP. Specifically, for a 0.75% reinforcement ratio, ARCP-1 achieves an impressive reduction of approximately 24%, while ARCP-2 achieves an even more substantial reduction of about 33%. This reduction in reinforcement quantity can be even more pronounced when the distance between the partial surface saw-cuts surpasses 1200 mm. Drawing upon field evidence derived from the active cracking experiments on the CRCP sections constructed in the United States and Belgium, as previously discussed, it is reasonable to infer that, for a given lane width of 1800 mm, the inclusion of 9 and 6 continuous-placed steel bars in ARCP-1 and ARCP-2, respectively, will adequately serve to restrain passive cracks that may develop in between the active cracks.

For a 0.85% steel ratio, the reinforcement layouts for ARCP using a 16 mm diameter steel bar are shown in Fig. 26. The choice of a 16 mm diameter steel bar aligns with the design concept-2 employed in CRCP projects in Belgium, where favorable cracking characteristics were observed⁵. Opting for a steel bar of 16 mm diameter,

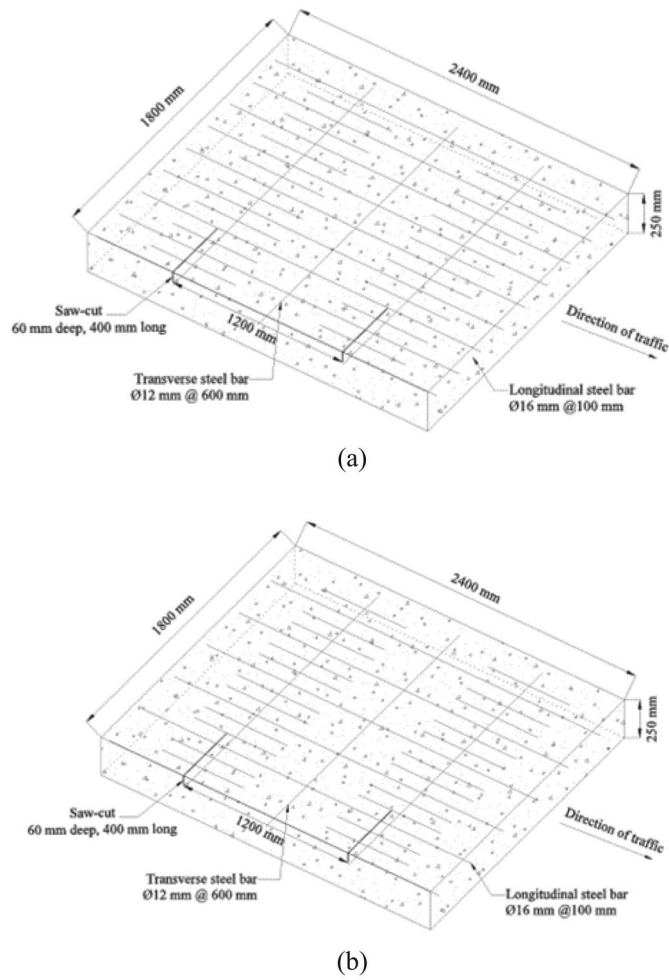


Figure 24. Configuration of reinforcement in ARCP with a 0.75% reinforcement ratio employing 16 mm diameter steel bars (a) ARCP-1 (b) ARCP-2.

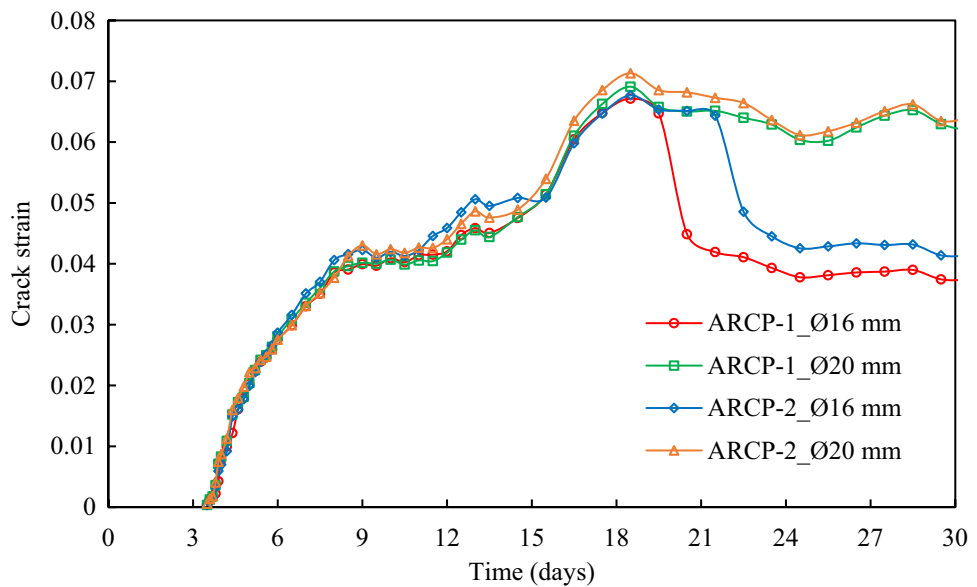


Figure 25. Crack strain evolution at the notch tip in ARCP-1 and ARCP-2 with a 0.75% steel ratio employing 16 mm and 20 mm steel bar diameters.

| Layout design | CRCP | ARCP-1 | ARCP-2 |
|------------------------------------------------|-------|--------|--------|
| Slab width (mm) | 1800 | 1800 | 1800 |
| Slab length (mm) | 2400 | 2400 | 2400 |
| Saw-cut spacing (mm) | 1200 | 1200 | 1200 |
| Continuous-length steel bar diameter (mm) | 20 | 16 | 16 |
| Continuous-length steel bar length (mm) | 2400 | 2400 | 2400 |
| Number of continuous-length steel bar rows | 11 | 9 | 6 |
| Steel ratio at active crack locations (%) | 0.75 | 0.75 | 0.75 |
| Partial-length steel bar diameter (mm) | – | 16 | 16 |
| Partial-length steel bar length (mm) | – | 600 | 600 |
| Number of partial-length steel bar rows | – | 8 | 11 |
| Steel ratio between active crack locations (%) | 0.75 | 0.40 | 0.27 |
| Total amount of steel (kg/m ³) | 60.37 | 45.64 | 40.37 |
| Steel reduction relative to CRCP (%) | – | 24.39 | 33.12 |

Table 4. Comparison of reinforcement layout of ARCP design with those of the CRCP design for 0.75% steel ratio.

rather than a 20 mm one with the same reinforcement ratio and geometric configuration, offers potential benefits due to the increased number of continuous-placed steel bars associated with smaller bar diameters. As stated before, the primary function of continuous-placed steel bars in the CRCP is to securely keep cracks together. Consequently, adding more continuous steel bars will enhance the continuity of the pavement construction.

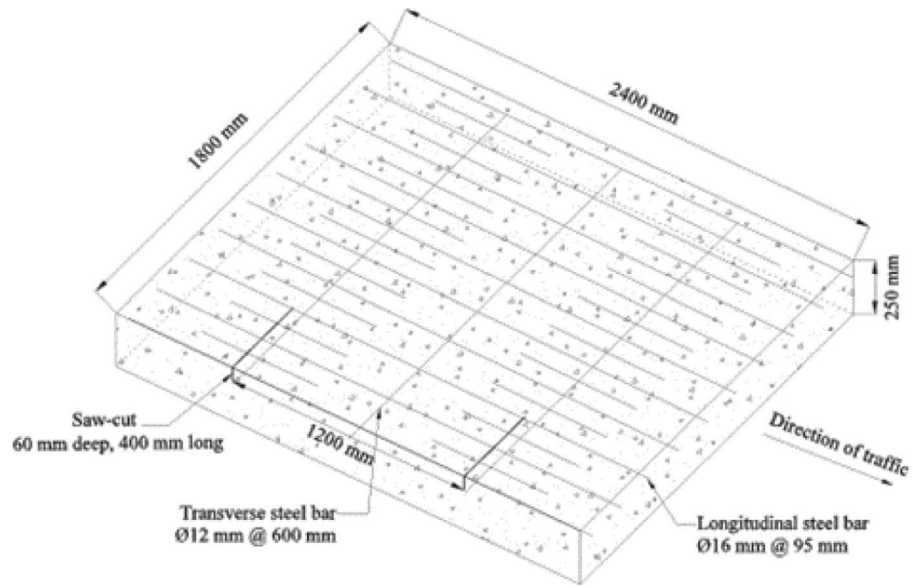
Figure 27 illustrates the evolution of crack strain over time at the notch tip for both ARCP-1 and ARCP-2. As depicted in Fig. 27, ARCP-1 exhibits lower values of the crack strain than ARCP-2 for a 0.85% reinforcement ratio. This observation suggests that an increase in the number of continuous-length steel bars within the ARCP leads to a reduction in crack strain. The above-mentioned findings indicate that much like in the case of the CRCP slab, active cracking could play a critical role in influencing the long-term performance of the ARCP slab. Furthermore, a notable advantage emerges when evaluating ARCP with a higher reinforcement ratio of 0.85% against CRCP structures with a 0.75% reinforcement ratio, as detailed in Table 5. ARCP achieves substantial reductions of approximately 16% and 24% in total steel consumption, underscoring its potential as a more resource-efficient alternative.

The reinforcement layout of the ARCP slab is also assessed using a reduced reinforcement ratio of 0.67%, used in design concept-2 for CRCP in Belgium^{5,16,43–46}. For this ratio, the reinforcement layouts of the ARCP slab using a 16 mm diameter steel bar are illustrated in Fig. 28. Figure 29 compares the time-dependent crack strain evolution between ARCP-1 and ARCP-2 at saw-cut tip with a 0.67% reinforcement ratio. Interestingly, there's no substantial difference in crack strain, likely due to the lower number of continuous-length steel bars compared to higher reinforcement ratios. This suggests that achieving the intended objective of maintaining pavement structure continuity, encompassing both passive and active cracks, may not be realized with a lower steel ratio of 0.67% in the ARCP slab design. Adopting ARCP-2 can lead to significant reinforcement savings, up to 42%, as detailed in Table 6, particularly if partial surface saw-cuts effectively induce active cracking. These research findings provide valuable insights for planning field trial sections, contributing to a more logically grounded structural design for ARCP slabs.

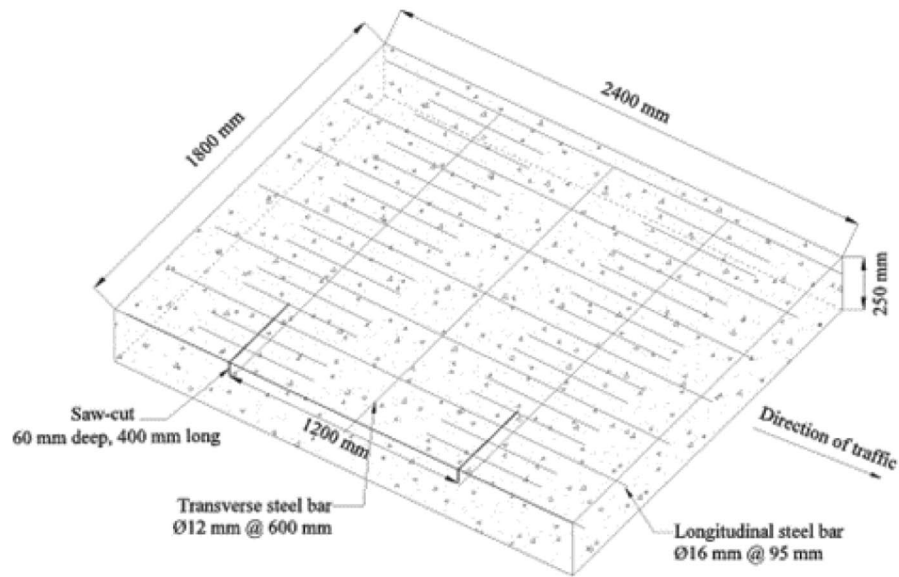
Discussion

Continuous steel bars within the CRCP slab serve to maintain structural continuity by tightly coupling cracks, thus preventing excessive crack expansion. This inherent continuity, however, leads to a higher initial construction cost compared to traditional concrete pavements. The behavior of CRCP in the early phases, when issues like punch-out and spalling are predominantly connected to non-uniform cracking patterns, especially clusters of closely spaced cracks, determines much of its long-term performance. Achieving predictability in transverse crack patterns remained a persistent challenge despite numerous attempts such as changing reinforcement ratio, steel depth, aggregate type, and slab thickness. In Belgium, the precise control of crack locations in CRCP has been successfully achieved through the implementation of partial surface saw cuts. This proactive method for controlling cracks is now being adopted in the United States to intentionally induce desired crack patterns in CRCP test sections^{8,18}.

The transformation of a CRCP slab into an ARCP slab involves inducing active cracking by eliminating superfluous continuous steel bars located between active cracks and replacing the continuous steel bars originally intended to span those cracks with partial steel bars. Drawing from comprehensive field investigations carried out on existing CRCP sections in both Belgium and the United States, the ARCP design offers a viable alternative to the CRCP design, substantially reducing the required reinforcement while preserving the fundamental performance characteristics of CRCP. In Belgium, the current CRCP design concept-3 can be adapted to the ARCP design employing the ARCP-2 layout, leading to a potential reduction in reinforcement by up to 33%. Nevertheless, the performance of ARCP, including post-cracking behavior and crack width variations, must be observed over a two-year period encompassing a complete environmental cycle through the implementation of field trial sections. The installation of partial steel bars at transverse steel locations may present greater challenges



(a)



(b)

Figure 26. Configuration of reinforcement in ARCP with a 0.85% reinforcement ratio employing 16 mm diameter steel bars (a) ARCP-1 (b) ARCP-2.

compared to the conventional continuous bar placement method. To address this, two transverse steel bars can be strategically positioned at the ends of the partial steel bar to provide support for longitudinal reinforcement in ARCP. In this configuration, the spacing between the transverse steel bars aligns with the overall length of the partial steel bar. Furthermore, the automated tape insertion method and internal curing could be combined with partial surface saw-cuts to accelerate the induction of active cracking in the ARCP slab, further minimizing the steel content.

Summary of findings

The efficiency of the active cracking method to generate controlled cracks over specified areas of the concrete slab where continuous-length steel bars are partially substituted with partial-length steel bars determines the reinforcing layout of the ARCP. This study aims to optimize the reinforcement layout of the ARCP slab for

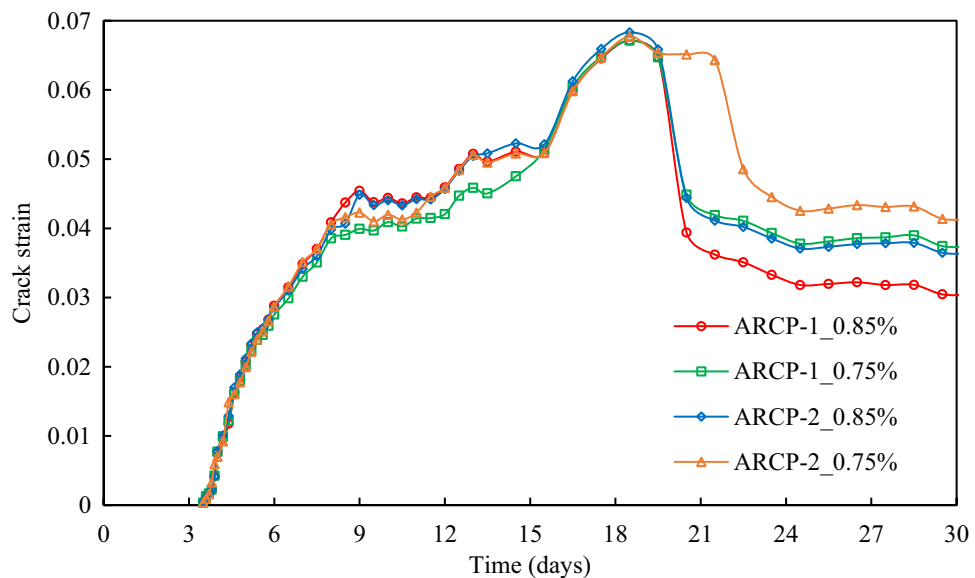
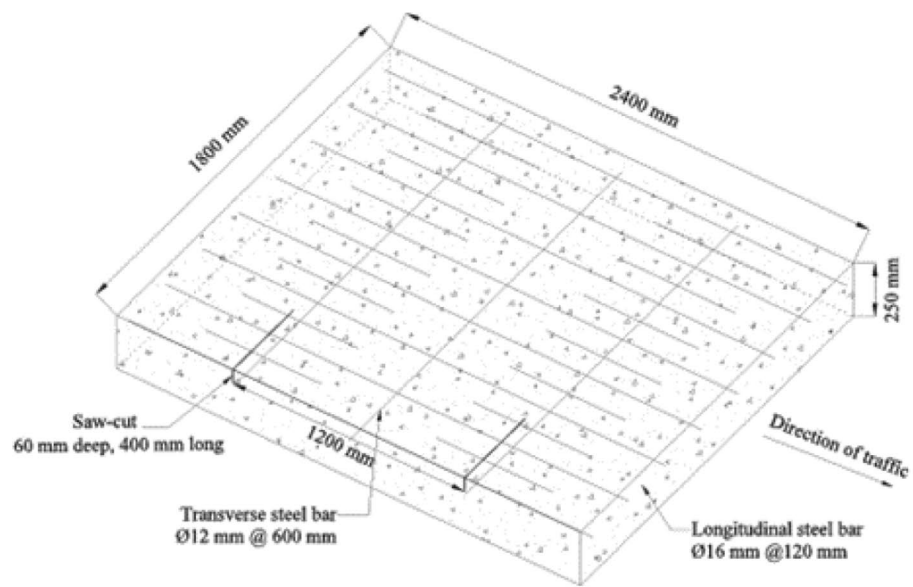


Figure 27. Crack strain evolution at the notch tip in ARCP-1 and ARCP-2 with 0.75% and 0.85% reinforcement ratios.

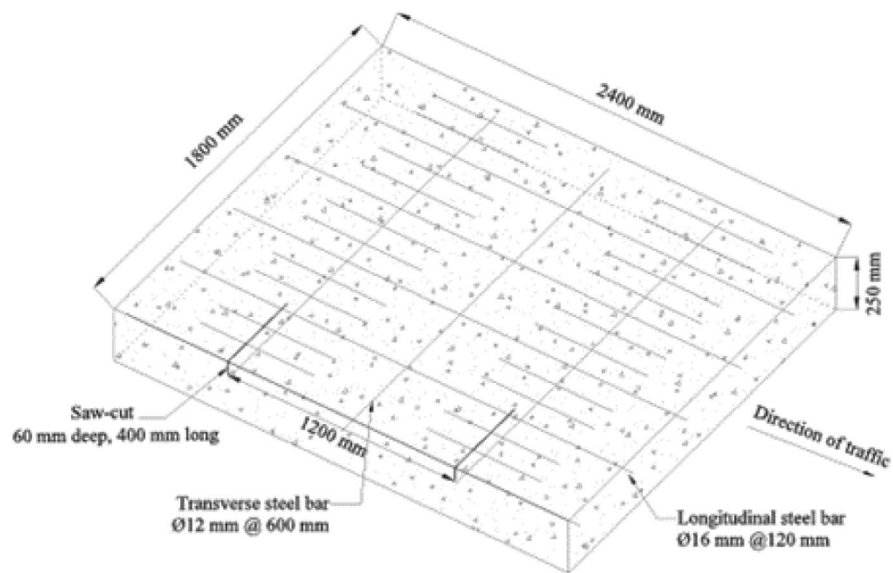
| Layout design | CRCP | ARCP-1 | ARCP-2 |
|------------------------------------------------|-------|--------|--------|
| Slab width (mm) | 1800 | 1800 | 1800 |
| Slab length (mm) | 2400 | 2400 | 2400 |
| Saw-cut spacing (mm) | 1200 | 1200 | 1200 |
| Continuous-length steel bar diameter (mm) | 20 | 16 | 16 |
| Continuous-length steel bar length (mm) | 2400 | 2400 | 2400 |
| Number of continuous-length steel bar rows | 11 | 10 | 7 |
| Steel ratio at active crack locations (%) | 0.75 | 0.85 | 0.85 |
| Partial-length steel bar diameter (mm) | – | 16 | 16 |
| Partial-length steel bar length (mm) | – | 600 | 600 |
| Number of partial-length steel bar rows | – | 9 | 12 |
| Steel ratio between active crack locations (%) | 0.75 | 0.45 | 0.313 |
| Total amount of steel (kg/m ³) | 60.37 | 50.91 | 45.64 |
| Steel reduction relative to CRCP (%) | – | 15.67 | 24.4 |

Table 5. Comparison of reinforcement layout details of ARCP design for a steel ratio of 0.85% with those of the CRCP design having 0.75% steel ratio.

various steel ratios by developing a FE model, thereby circumventing the need for resource-intensive field trials. The results derived from the FE simulations are validated through on-site observations of active cracking in CRCP test sections. The evaluation of reinforcement layouts for the ARCP slab primarily focuses on early-age crack induction and the amount of reinforcement used, in comparison to CRCP slabs designed with steel ratios of 0.85%, 0.75%, and 0.67% as applied in design concepts 1 through 3 in Belgium. The current CRCP design in Belgium is compared with two basic ARCP reinforcement layout concepts referred to as ARCP-1 (replacement of every successive continuous-length steel bar with a partial-length steel bar) and ARCP-2 (replacement of every two consecutive continuous-length steel bars with partial-length steel bars). Notably, for a steel ratio of 0.75%, ARCP-1 and ARCP-2 lead to reductions of reinforcement to 24% and 33%, respectively, compared to CRCP. This reduction in reinforcement escalates to 33% and 42% in ARCP-1 and ARCP-2, respectively, when considering a 0.67% steel ratio. Even at a steel ratio of 0.85%, ARCP facilitates a reduction in reinforcement by up to 15% and 24% in ARCP-1 and ARCP-2, respectively, relative to CRCP. It is important to highlight that ARCP represents an innovative rigid pavement structure that has not yet been constructed. To comprehensively apprehend its cracking behavior and variations in crack width over an entire environmental cycle, the establishment of field trial test sections is imperative. The insights obtained from this study can offer valuable preliminary guidance for the development of an ARCP slab with a structurally optimized design.



(a)



(b)

Figure 28. Configuration of reinforcement in ARCP with a 0.67% reinforcement ratio using 16 mm diameter steel bars (a) ARCP-1 (b) ARCP-2.

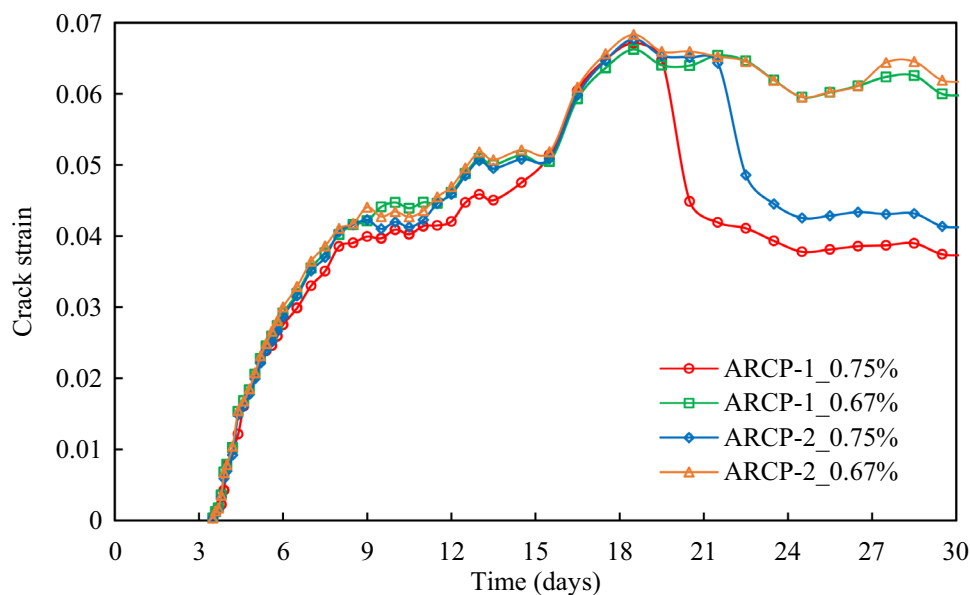


Figure 29. Crack strain evolution at the notch tip in ARCP-1 and ARCP-2 with 0.67% and 0.75% reinforcement ratios.

| Layout design | CRCP | ARCP-1 | ARCP-2 |
|------------------------------------------------|-------|--------|--------|
| Slab width (mm) | 1800 | 1800 | 1800 |
| Slab length (mm) | 2400 | 2400 | 2400 |
| Saw-cut spacing (mm) | 1200 | 1200 | 1200 |
| Continuous-length steel bar diameter (mm) | 20 | 16 | 16 |
| Continuous-length steel bar length (mm) | 2400 | 2400 | 2400 |
| Number of continuous-length steel bar rows | 11 | 8 | 5 |
| Steel ratio at active crack locations (%) | 0.75 | 0.75 | 0.75 |
| Partial-length steel bar diameter (mm) | – | 16 | 16 |
| Partial-length steel bar length (mm) | – | 600 | 600 |
| Number of partial-length steel bar rows | – | 7 | 10 |
| Steel ratio between active crack locations (%) | 0.75 | 0.36 | 0.22 |
| Total amount of steel (kg/m ³) | 60.37 | 40.37 | 35.11 |
| Steel reduction relative to CRCP (%) | – | 33.12 | 41.84 |

Table 6. Comparison of reinforcement layout details of the ARCP design for a steel ratio of 0.67% with those of the CRCP design having 0.75% steel ratio.

Data availability

Data is contained within the article or supplementary material: further inquiries can be directed to the corresponding author.

Received: 18 May 2024; Accepted: 23 July 2024

Published online: 28 July 2024

References

- Kim, S.-M., Cho, Y. K. & Lee, J. H. Advanced reinforced concrete pavement: Concept and design. *Constr. Build. Mater.* **231**, 117130 (2020).
- Kashif, M., et al. Early-age cracking behavior of advanced reinforced concrete pavement under environmental loading. in *IABSE Congress: Structural Engineering for Future Societal Needs*. 2021. International Association for Bridge and Structural Engineering (IABSE).
- Kashif, M. et al. Evaluating the early-age crack induction in advanced reinforced concrete pavement using partial surface saw-cuts. *Appl. Sci.* **11**(4), 1659 (2021).
- Ouzaa, K. & Benmansour, M. B. Cracks in continuously reinforced concrete pavement. *Arab. J. Sci. Eng.* **39**(12), 8593–8608 (2014).
- Ren, D., *Optimisation of the Crack Pattern in Continuously Reinforced Concrete Pavements*. 2015, Ph.D. Thesis, Technische Universiteit Delft, The Netherlands.
- Kim, K. et al. Optimization of parameters affecting horizontal cracking in continuously reinforced concrete pavement (CRCP). *Can. J. Civ. Eng.* **46**(7), 634–642 (2019).

7. Citir, N. *et al.* Investigation of factors affecting distresses on continuously reinforced concrete pavement using ground penetrating radar. *J. Perform. Constr. Facil.* **34**(3), 04020027 (2020).
8. Dahal, S. & Roesler, J. R. Continuously reinforced concrete pavement cracking patterns and properties with internal curing and active cracking. *Transp. Res. Record* **2676**(2), 325–333 (2022).
9. Liu, K. *et al.* Laboratory investigation on early-age shrinkage cracking behavior of partially continuous reinforced concrete pavement. *Constr. Build. Mater.* **377**, 131125 (2023).
10. Tayabji, S. D. *et al.* *Performance of Continuously Reinforced Concrete Pavements. Volume III-Analysis and Evaluation of Field Test Data.* Department of Transportation. Federal Highway Administration. Office of Research and Development; Turner-Fairbank Highway Research Center: The United States (1998).
11. Zollinger, D., *et al.*, *Performance of CRCP volume 6-CRCP design, construction, and performance.* FHWA-RD-97-151, Report, Washington, DC (1998).
12. McCullough, B. F. & Dossey, T. Considerations for high-performance concrete paving: Recommendations from 20 years of field experience in Texas. *Transp. Res. Record* **1684**(1), 17–24 (1999).
13. McCullough, B.F., Zollinger, D. & Dossey, T. *Evaluation of the Performance of Texas Pavements Made with Different Coarse Aggregates.* University of Texas at Austin. Center for Transportation Research: University of Texas at Austin. Center for Transportation Research (2000).
14. Kohler, E. & Roesler, J. Active crack control for continuously reinforced concrete pavements. *Transp. Res. Record* **1900**(1), 19–29 (2004).
15. Kohler, E. & Roesler, J. Crack spacing and crack width investigation from experimental CRCP sections. *Int. J. Pavement Eng.* **7**(4), 331–340 (2006).
16. Ren, D. *et al.* Active crack control for continuously reinforced concrete pavements in Belgium through partial surface notches. *Transp. Res. Record* **2456**(1), 33–41 (2014).
17. Kashif, M. *et al.* Numerical evaluation of early-age crack induction in continuously reinforced concrete pavement with different Saw-cut dimensions subjected to external varying temperature field. *Appl. Sci.* **11**(1), 42 (2020).
18. Roesler, J. *et al.* *Summary Findings of Re-engineered Continuously Reinforced Concrete Pavement: Volume 1.* University of Illinois at Urbana-Champaign. Department of Civil and Environmental Engineering; Texas A & M University; Oregon State University, (2021).
19. Lee, H. *et al.* *Optimizing Reinforcing Steel in 12-in and 13-in Continuously Reinforced Concrete Pavement (CRCP).* Texas Tech University. Center for Multidisciplinary Research in Transportation, (2023).
20. Kim, S.-M., Won, M. & Frank McCullough, B. Numerical modeling of continuously reinforced concrete pavement subjected to environmental loads. *Transp. Res. Record* **1629**(1), 76–89 (1998).
21. Kim, S.-M., Won, M. C. & Frank McCullough, B. Three-dimensional analysis of continuously reinforced concrete pavements. *Transp. Res. Record* **1730**(1), 43–52 (2000).
22. Al-Qadi, I. & Elseifi, M. Mechanism and modeling of transverse cracking development in continuously reinforced concrete pavement. *Int. J. Pavement Eng.* **7**(4), 341–349 (2006).
23. Choi, S. *et al.* *Horizontal Cracking Mechanism in CRCP.* (2009).
24. Choi, S., Ha, S. & Won, M. C. Horizontal cracking of continuously reinforced concrete pavement under environmental loadings. *Constr. Build. Mater.* **25**(11), 4250–4262 (2011).
25. Choi, S., Ha, S. & Won, M. C. Mechanism of transverse crack development in continuously reinforced concrete pavement at early ages. *Transp. Res. Record* **2524**(1), 42–58 (2015).
26. Choi, S., Na, B.-U. & Won, M. C. Mesoscale analysis of continuously reinforced concrete pavement behavior subjected to environmental loading. *Constr. Build. Mater.* **112**, 447–456 (2016).
27. Kashif, M. *et al.* Three dimensional finite element model for active crack control in continuously reinforced concrete pavement. in *Proceedings of the 9th International Conference on Maintenance and Rehabilitation of Pavements—Mairepav9.* 2020. Springer.
28. Diana, F. & D.U.s. Manual, *Release 10.3*, in *Diana FEA: Delft, The Netherlands.* 2019.
29. Standard, E., EN 1992-1-1: 2004 Eurocode 2: Design of concrete structures, in *Part 1-1: General Rules and Rules for Buildings,* (1992).
30. Hendriks, M. A. & Rots, J. *Finite Elements in Civil Engineering Applications: Proceedings of the Third Diana World Conference, Tokyo, Japan, 9–11 October 2002.* 2002: CRC Press.
31. Byfors, J. *Plain Concrete at Early Ages.* (1980).
32. Neville, A. M. & Brooks, J. J. *Concrete Technology* Vol. 438 (Longman Scientific & Technical, England, 1987).
33. Khan, A. A., Cook, W. D. & Mitchell, D. Thermal properties and transient thermal analysis of structural members during hydration. *Mater. J.* **95**(3), 293–303 (1998).
34. De Schutter, G. *Thermal Properties, Early Age Cracking in Cementitious Systems.* 2001, Report 25, A. Bentur, RILEM Publications sar 1., 121–126, (2001).
35. Morabito, P. *Thermal Properties of Concrete: Variations with the Temperature and During the Hydration Phase* (Department of Civil & Mining Engineering & Division of Structural Engineering, 2001).
36. Faria, R., Azenha, M. & Figueiras, J. A. Modelling of concrete at early ages: Application to an externally restrained slab. *Cement Concr. Compos.* **28**(6), 572–585 (2006).
37. Saeed, M. K., Rahman, M. K. & Baluch, M. H. Early age thermal cracking of mass concrete blocks with Portland cement and ground granulated blast-furnace slag. *Mag. Concr. Res.* **68**(13), 647–663 (2016).
38. Kada, H. *et al.* Determination of the coefficient of thermal expansion of high performance concrete from initial setting. *Mater. Struct.* **35**, 35–41 (2002).
39. Narin, F. & Wiklund, O. *Design of slabs-on-ground regarding shrinkage cracking.* 2012.
40. Mapa, D. G. *et al.* Evaluating early-age stresses in jointed plain concrete pavement repair slabs. *ACI Mater. J.* **117**(4), 119–132 (2020).
41. Sofi, M. *et al.* Influence of ambient temperature on early age concrete behaviour of anchorage zones. *Constr. Build. Mater.* **53**, 1–12 (2014).
42. Sofi, M. *et al.* Thermal stresses of concrete at early ages. *J. Mater. Civ. Eng.* **31**(6), 04019056 (2019).
43. Verhoeven, K. Cracking and corrosion in continuously reinforced concrete pavements. in *Fifth International Conference on Concrete Pavement Design and Rehabilitation* Purdue University, School of Civil Engineering; Federal Highway Administration; Portland Cement Association; Transportation Research Board; Indiana Department of Transportation; Federal Aviation Administration; and American Concrete Pavement Association, (1993).
44. Beeldens, A. & Rens, L. The behaviour of CRCP in Belgium: Observation and measurement of crack pattern, bond and thermal movement. in *7th International DUT-Workshop on Design and Performance of Sustainable and Durable Concrete Pavements, Date: 2010/01/10–2010/01/11, Location: Seville (Spain),* (2010).
45. Ren, D., Houben, L. & Rens, L. Cracking behavior of continuously reinforced concrete pavements in Belgium: Characterization of current design concept. *Transp. Res. Record* **2367**(1), 97–106 (2013).
46. Ren, D., Houben, L. J. & Rens, L. Monitoring early-age cracking of continuously reinforced concrete pavements on the E17 at Ghent (Belgium), in *Sustainable Construction Materials 2012.* 30–41, (2013).

Acknowledgements

The authors gratefully acknowledge the financial assistance (HRDIUESTP/UETs Phase 1) for the CRCP project from The Higher Education Commission (HEC), Pakistan, and the research facilities provided by Ghent University, Belgium.

Author contributions

Conceptualization, M.K. and P.W.; methodology, M.K.; software, A.H.; validation, M.K., A.N. and H.B.; formal analysis, M.R.; investigation, S.M.; resources, K.O.; data curation, P.W.; writing—original draft preparation, M.K.; writing—review and editing, A.N.; visualization, K.O.; supervision, H.B.; project administration, P.W.; funding acquisition, K.O. All authors have read and agreed to the submitted version of the manuscript.

Competing interests

The authors declare no competing interests.

Additional information

Correspondence and requests for materials should be addressed to K.C.O.

Reprints and permissions information is available at www.nature.com/reprints.

Publisher's note Springer Nature remains neutral with regard to jurisdictional claims in published maps and institutional affiliations.



Open Access This article is licensed under a Creative Commons Attribution-NonCommercial-NoDerivatives 4.0 International License, which permits any non-commercial use, sharing, distribution and reproduction in any medium or format, as long as you give appropriate credit to the original author(s) and the source, provide a link to the Creative Commons licence, and indicate if you modified the licensed material. You do not have permission under this licence to share adapted material derived from this article or parts of it. The images or other third party material in this article are included in the article's Creative Commons licence, unless indicated otherwise in a credit line to the material. If material is not included in the article's Creative Commons licence and your intended use is not permitted by statutory regulation or exceeds the permitted use, you will need to obtain permission directly from the copyright holder. To view a copy of this licence, visit <http://creativecommons.org/licenses/by-nc-nd/4.0/>.

© The Author(s) 2024